



Research Article

Evaluation of Zn Adenine-Based Bio-MOF for Efficient Remediation of Different Types of Dyes

Eslam Salama ¹, Ali Hamdy,^{2,3} Hassan S. Hassan,^{4,5} Wael A. Amer ^{2,6},
El-Zeiny M. Ebeid,^{2,7} Mona Ossman,¹ and Marwa F. Elkady^{8,9}

¹Environment and Natural Materials Research Institute (ENMRI), City of Scientific Research and Technological Applications (SRTA-City), New Borg El-Arab City, Alexandria 21934, Egypt

²Chemistry Department, Faculty of Science, Tanta University, Tanta 31527, Egypt

³Environmental Biotechnology Department, Genetic Engineering and Biotechnological Research Institute (GEBRI), City of Scientific Research and Technological Applications (SRTA-City), New Borg El-Arab City, Alexandria 21934, Egypt

⁴Electronic Materials Research Department, Advanced Technology and New Materials Research Institute (ATNMRI), City of Scientific Research and Technological Applications (SRTA-City), New Borg El-Arab City, Alexandria 21934, Egypt

⁵Environmental Engineering Department, Egypt-Japan University of Science and Technology, New Borg El-Arab City, Alexandria 21934, Egypt

⁶Department of Chemistry, College of Science, University of Bahrain, Sakhir 32038, Bahrain

⁷Center of Basic Sciences (CBS), Misr University for Science and Technology (MUST), 6th of October City 12563, Egypt

⁸Fabrication Technology Research Department, Advanced Technology and New Materials Research Institute (ATNMRI), City of Scientific Research and Technological Applications (SRTA-City), New Borg El-Arab City, Alexandria 21934, Egypt

⁹Chemical and Petrochemical Engineering Department, Egypt-Japan University of Science and Technology (E-JUST), New Borg El-Arab City, Alexandria 21934, Egypt

Correspondence should be addressed to Eslam Salama; eslamsobhysalama@gmail.com

Received 6 January 2022; Revised 10 July 2022; Accepted 2 August 2022; Published 13 August 2022

Academic Editor: Adrián Bonilla-Petriciolet

Copyright © 2022 Eslam Salama et al. This is an open access article distributed under the Creative Commons Attribution License, which permits unrestricted use, distribution, and reproduction in any medium, provided the original work is properly cited.

As an eco-friendly material, Zn-adeninate bio-metal-organic framework (bio-MOF) was investigated as an efficient adsorbent for both anionic and cationic dyes. The adsorption capability of the synthesized Zn-adeninate bio-MOF was confirmed by its notable surface area of $52.62 \text{ m}^2 \text{ g}^{-1}$ and total pore volume of $0.183 \text{ cm}^3 \text{ g}^{-1}$. The bio-MOF adsorption profiles of anionic direct red 81 (DR-81) and cationic methylene blue (MB) dyes were investigated under different operating parameters. The optimum dosages of Zn-adeninate bio-MOF were 0.5 g L^{-1} and 1 g L^{-1} for MB and DR-81 decolorization, respectively. The pH_{PZC} of Zn-adeninate bio-MOF was 7.2, and maximum monolayer adsorption capacity was 132.15 mg g^{-1} for MB, which decreased to 82.54 mg g^{-1} for DR-81 dye. Thermodynamic data indicated the spontaneous and endothermic nature of the decolorization processes. Additionally, the adsorption processes were in agreement with the Langmuir and pseudo-second-order kinetic models. The synthesized Zn-adeninate bio-MOF could be reused several times with high decolorization ability. These findings demonstrated that the synthesized Zn bio-MOF is an effective and promising adsorbent material for the removal of both cationic and anionic dyes from polluted water.

1. Introduction

Water accounts for approximately 70% of the Earth's surface, but only approximately 3% is freshwater. A large fraction of the freshwater is locked up in glacial ice caps or at great depths under the surface of the earth, which is difficult

to extract and hence is not used by humans. Moreover, a high percentage of the freshwater has become highly polluted, leaving only 0.4% as usable, which is insufficient for the 7.80 billion people living on the earth [1]. The safety of water sources is the most challenging matter related to water sustainability that is faced by several countries worldwide.

Contamination of water with harmful materials, such as organic dyes and heavy metal ions, is a severe problem because of their toxic and carcinogenic nature [2].

Currently, a large number of fabricated dyes are produced annually around the globe, and approximately 10% of these are discharged into the environment as wastewater because they (50% concentration) do not strictly bind to the fibers and can act as liquid contaminants [3]. Additionally, the multifaceted aromatic structures of the synthetic dyes make them stable and difficult to decompose [4]. The aromatic amines created after the degradation of azo dyes, a type of synthetic dye, are highly toxic [5]. Moreover, approximately 40% of the dyes contain organically bound chlorine, which is a known carcinogen [6]. Further, the discharge of dye-polluted liquids into streams and rivers lowers dissolved oxygen and enables anaerobic media, which can destroy aquatic organisms [4].

Direct dyes are characterized by their affinity for bleached and unbleached chemical pulps and are primarily used in the pulp and textile industries. They usually contain sulfonic acid groups and at least one azo group that imparts water solubility to the dyes. Direct red-81 dye (DR-81) is one of the most famous anionic azo dyes used in industrial applications (Figure 1(a)) [7]. By contrast, methylene blue (3,7-bis(dimethylamino)-phenothiazin-5-ium chloride) (MB) or basic blue-9 is a univalent cationic dye with the molecular formula of $C_{16}H_{18}N_3ClS$, as shown in Figure 1(b), and is utilized for biological staining as well as coloring hair, papers, wool, and cotton [8]. However, the accumulation of MB in water has undesirable health effect, including eye burns, breathing problems, diarrhea, and nausea [9].

Accordingly, researchers have investigated various techniques for wastewater treatment, such as advanced oxidation processes [10], electrocoagulation, coagulation/flocculation [11], adsorption [12–14], activated sludge processes [15], filtration [16], ion exchange [17], photodegradation [18], membrane bioreactors [19], bed biofilm reactors [20], and constructed wetlands (CW) [21]. Among these techniques, adsorption is a very efficient removal technique because of its ease of operation, high removal efficiency, reusability of the adsorbents, and cost-effectiveness. Adsorption involves transition of solids from the solution to the adsorbent surface [22]. Several adsorbents, such as carbon-based nano-adsorbents, polymer-based adsorbents, biosorbents, transition metal-based oxides, and metal-organic frameworks (MOFs), have been employed to remove dyes from wastewater [1, 23–25]. Recent studies have found that MOFs are powerful adsorbents compared to other materials owing to their high surface areas and porous structures [1, 26].

MOFs are a category of hybrid materials that contain metal ion-based matrices and organic ligands that attach the vertices to form two- or three-dimensional periodic structures [1]. The appropriate choice of organic ligands and vertices results in the synthesis of MOFs with different pore sizes, topologies, and geometries. Several techniques, such as defect engineering, modulation of noncovalent interactions, and functionalization of organic ligands [26], have been developed to prepare porous frameworks for adsorbing organic dyes with high selectivity. Significant advancements

have been made in the design of water-stable MOFs. MOFs can be soaked in water for extended periods at various pH values without changing their structures [27]. Consequently, MOFs are considered promising materials for wastewater remediation owing to their impressive properties and specific interactions with the pollutants, in addition to their catalytic activities against specific organic pollutants [28].

In recent years, bio-MOFs have attracted significant interest as green sustainable frameworks. Derived biomolecules that are usually readily biodegradable and nontoxic are combined to synthesize bio-MOFs [1, 29]. Biomolecules, such as polysaccharides, amino acids, nucleobases, and peptides, are combined with metal ions to synthesize bio-MOFs. Salamat et al. studied the combination of a polysaccharide with metal ions for MOF crystallization under biocompatible conditions. The hydroxyl groups present on the polysaccharide molecules were found to assist in the coordination interactions with the metal ions. Hence, functional polysaccharides trigger the formation of MOFs by controlling the morphological structure and particle size of the prepared MOFs [30]. Furthermore, the integration of the functionalized biopolymers with MOF materials can improve the biocompatibility, adsorption, and flexibility of the composite materials, which can extend their application in biocatalysis and biological sciences [31]. Zn-based bio-MOFs have been used for the wastewater remediation because of their high porosity, which simplifies the decontamination process of pollutants [1]. The existence of tunable chemical functions, such as $-NH_2$ groups, result in excellent removal capacities of the negative and positive dyes [32]. In this study, an eco-friendly reusable Zn-adeninate bio-MOF was synthesized and investigated as an effective adsorbent material for the anionic DR-81 and cationic MB dyes from polluted water.

2. Materials and Methods

2.1. Materials. Adenine and 4,4'-biphenyl dicarboxylic acid were purchased from Alfa Aesar and Acros Organics, respectively. Zinc acetate dihydrate and dimethylformamide (DMF, HPLC) were obtained from Fisher Scientific. DR-81 (MW = 675.60 g mol⁻¹) and MB (MW = 319.85 g mol⁻¹) were procured from Sigma-Aldrich. The chemicals were used as received.

2.2. Synthesis of Zn-Adeninate Bio-MOF. In a 25 mL screw-capped tube, 0.03378 g of adenine was dispersed in 5 mL of DMF. The dispersed adenine powder was sonicated at 70°C for 6 h in an isothermal sonicator to obtain a well-dispersed solution of the organic ligand. In another 25 mL screw-capped tube, 0.1097 g of zinc acetate dihydrate was dissolved in 10 mL of DMF. Additionally, 0.12111 g of 4,4'-biphenyl dicarboxylic acid was dispersed in 6 mL of DMF, and all the tubes were sonicated in an isothermal sonicator for 6 h. Zinc acetate dihydrate solution was added to the dispersed adenine solution, and the dispersed 4,4'-biphenyl dicarboxylic acid solution was added to the mixture. Subsequently, 4 mL of DMF, 2 mL of methanol, and 0.5 mL of nanopure water were added to the mixture. Finally, the reaction mixture was heated

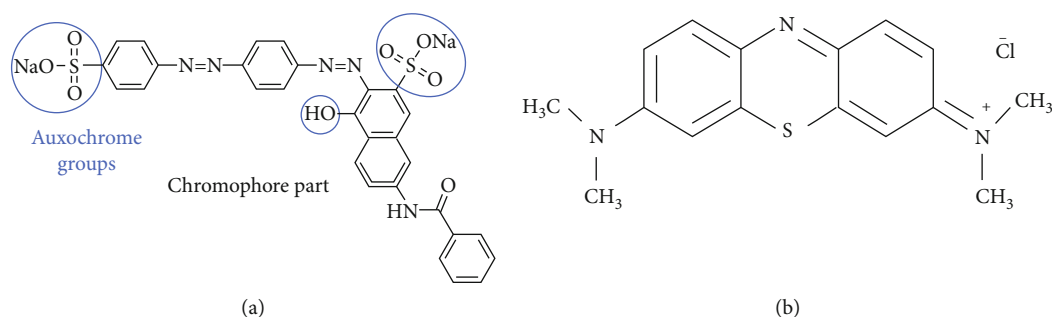


FIGURE 1: Structures of (a) direct red-81 and (b) methylene blue.

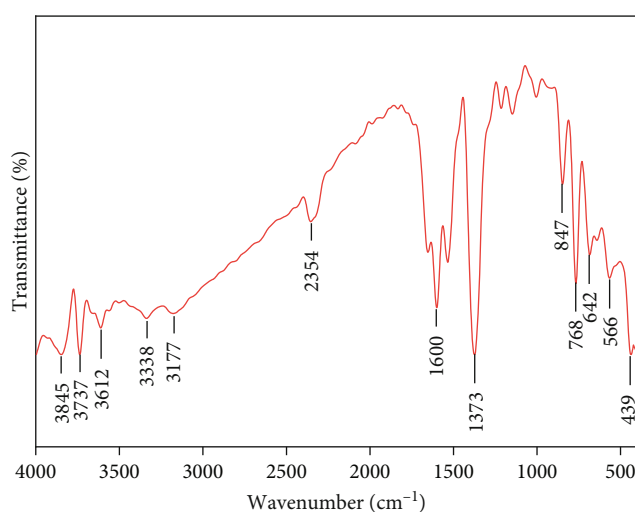


FIGURE 2: FTIR spectrum of the prepared Zn-adeninate bio-MOF.

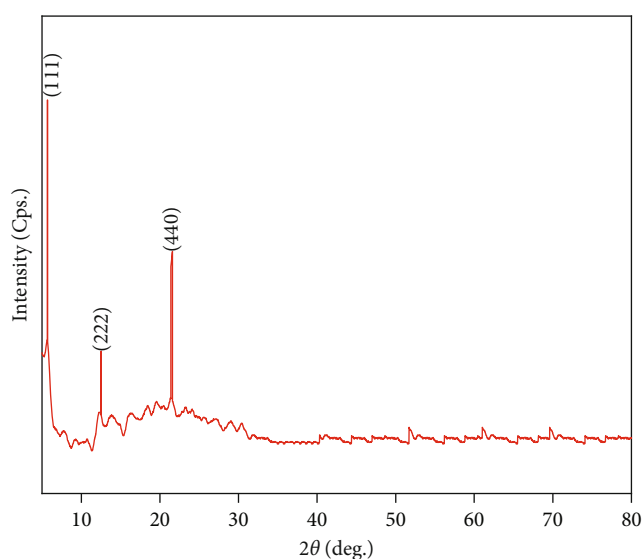


FIGURE 3: XRD pattern of the synthesized Zn-adeninate bio-MOF.

at 85°C for 24 h. After cooling to room temperature (23°C), the formed white precipitate was collected by centrifugation for 15 min at 6000 rpm, washed three times with 3 mL of DMF, and subsequently dried in an oven at 50°C overnight.

2.3. Characterization of the Synthesized Zn Bio-MOF. The functional groups of the synthesized Zn-adeninate bio-MOF were determined by analyzing its infrared absorption spectrum obtained using a Thermo Scientific Nicolet (USA). X-ray photoelectron spectroscopy (XPS, Thermo Fisher Scientific, USA) was used to evaluate the chemical states of the synthesized Zn-adeninate bio-MOF. To determine the crystal structure of the synthesized Zn-adeninate bio-MOF, X-ray diffraction (XRD) pattern of the synthesized sample was obtained by a Shimadzu XRD-6100 diffractometer with Cu-K α radiation at $\lambda = 1.54 \text{ \AA}$. Scanning electron microscopy (SEM, JEOL JSM-6010LV) was used to determine the morphology of the fabricated bio-MOFs. Transmission electron microscopy (TEM, JEOL JEM-2100F) was employed to obtain high-resolution images of the fabricated bio-MOF for investigating its bulk morphology. The pore size and surface area of the synthesized material were determined using a Belsorp-max automated apparatus via degassing of the fabricated Zn-adeninate MOF at 200°C for 6 h

before detection. The thermal stability of the fabricated bio-MOF was investigated using a TGA-50 (Shimadzu), and the weight loss of the material was recorded in the temperature range of 28–800°C under nitrogen gas atmosphere. The gas flow and material heating rates were 40 mL min⁻¹ and 10°C min⁻¹, respectively.

2.4. Decolorization of Cationic and Anionic Dyes using the Synthesized Bio-MOF. The characteristic adsorption affinity of the prepared Zn-adeninate bio-MOF was investigated for different pollutant dyes, including cationic and anionic dyes, using a batch technique. Subsequently, 50 mg of the synthesized Zn-adeninate bio-MOF was shaken at 23°C with 50 mL of the dye solution at different initial concentrations. The influence of adsorption parameters, such as pH (1–11), contact time (0–180 min), initial dye concentration (5–100 mg L⁻¹), material dosage (0.1–2 g L⁻¹), and reaction temperature (23–85°C), were investigated. The adsorption experiments were performed in triplicate to confirm the results, and the mean values were used for the data analysis. After the adsorption experiment, the supernatant was separated from the adsorbent material by centrifugation and

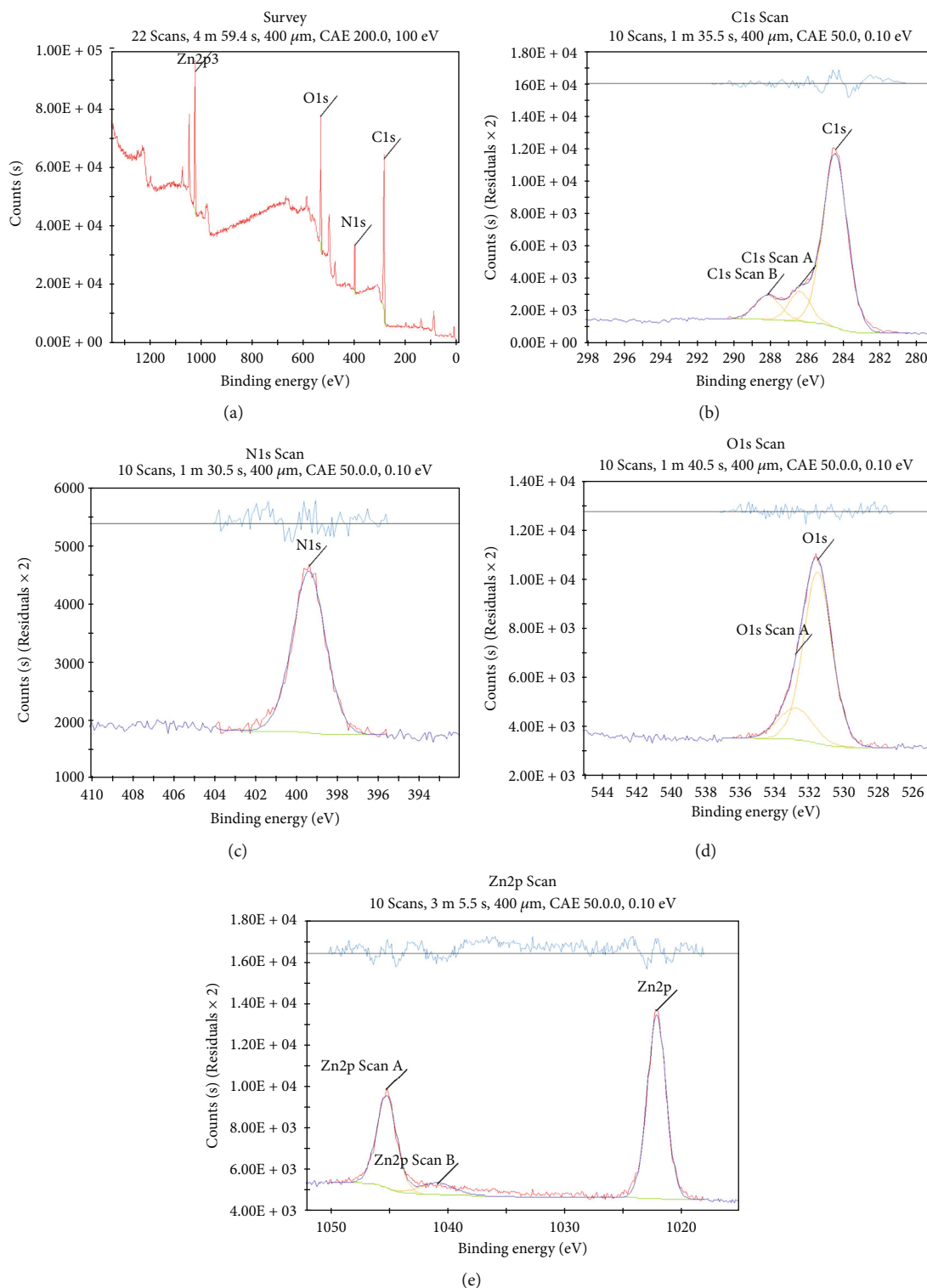


FIGURE 4: XPS spectra of the fabricated Zn-adeninate bio-MOF; (a) full spectrum, (b) C 1s spectrum, (c) N 1s spectrum, (d) O 1s spectrum, and (e) Zn 2p spectrum.

the absorbance of the supernatant was determined using a colorimetric method with a UV-visible spectrophotometer at 665 and 465 nm for MB and DR-81, respectively. The

decolorization percentage of the dye by the synthesized Zn-adeninate bio-MOF was calculated using the following equation [33]:

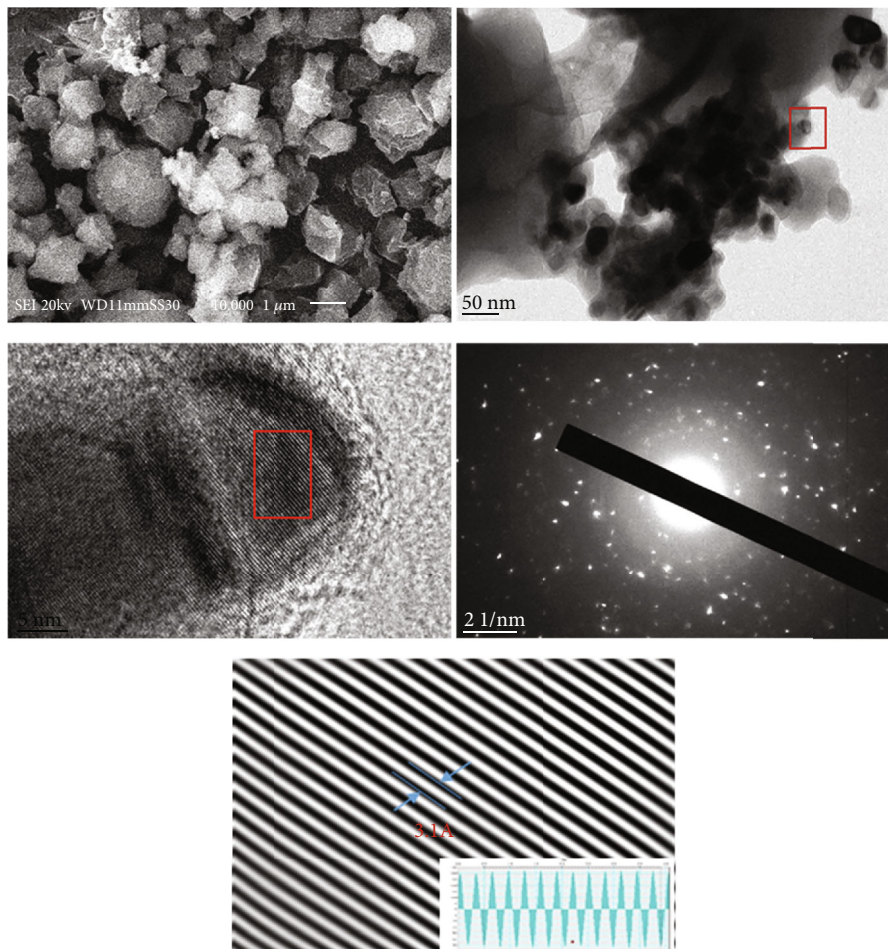


FIGURE 5: Morphological structures of the Zn-adeninate bio-MOF: (a) SEM and (b) TEM, HRTEM, fringe lattices, and SAED.

$$\text{Decolorization\%} = \left(\frac{C_o - C_e}{C_o} \right) \times 100, \quad (1)$$

where C_e and C_o refer to the equilibrium and initial pollutant concentrations (mgL^{-1}). The adsorption capacity (mg g^{-1}) was calculated using the following equation [13]:

$$q_e = \frac{V(C_o - C_e)}{m}, \quad (2)$$

where V denotes the solution volume (L), q_e denotes the adsorption capacity of the pollutant (mg g^{-1}), and m denotes the mass of the fabricated Zn-adeninate bio-MOF (g).

The point of zero charge of the synthesized Zn-adeninate bio-MOF was determined by mixing 0.1 g of the adsorbent material with 25 mL of 0.01 molar NaCl. The pH of the solution was adjusted to 1–12 using 0.01 M NaOH and/or 0.01 M HCl. Equilibration was achieved by shaking the solution in a thermostatic bath at 25°C for 24 h. The powdered material was separated, and the final pH of the supernatant was determined. The pH of the final solution was plotted against the initial pH, and the pH value at which the curves inter-

sected ($\text{pH}(\text{final}) = \text{pH}(\text{initial})$) was the pH_{pzc} of the fabricated Zn-adeninate bio-MOF [12].

2.5. Thermodynamics, Equilibrium, and Kinetics of the Bio-MOF Adsorption Behavior. The nature of the decolorization processes by the synthesized Zn-adeninate bio-MOF was evaluated by determining the thermodynamic parameters. The adsorption equilibrium was analyzed using the Langmuir, Freundlich, and Temkin isothermal models. Furthermore, the kinetics of the dye removal processes by the synthesized material were tested by applying the pseudo-first-order, pseudo-second-order, Elovich, and intraparticle kinetic models.

2.6. Regeneration of the Prepared Zn Bio-MOF. One gram of the used Zn-adeninate bio-MOF was recovered and washed three times with distilled water and 50 mL of methanol at 23°C, agitated at 150 rpm for 10 min, and dried at 150°C overnight for use in the subsequent adsorption experiments. Furthermore, the readsorption processes were performed at the following optimized removal conditions: *contact time* = 10 min for MB and 30 min for DR-81, *pH* = 7, *bio-MOF dosage* = 0.5 g L^{-1} for MB and 1 g L^{-1} for DR-

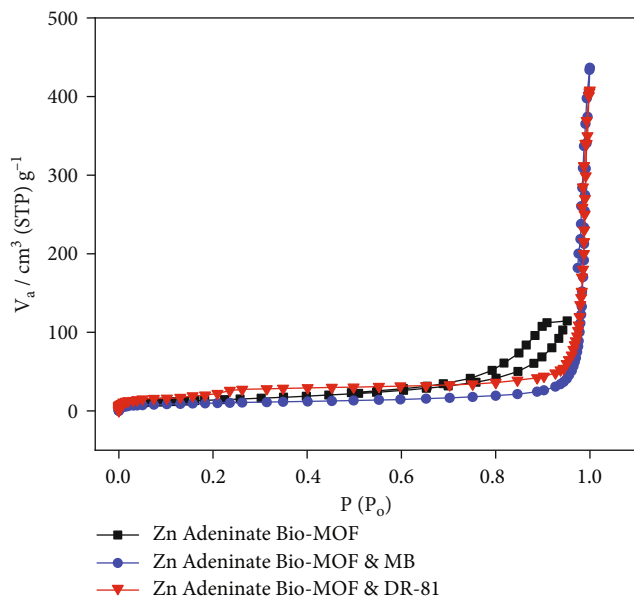


FIGURE 6: N_2 adsorption/desorption isotherm before and after decolorization of MB and DR-81 by the synthesized Zn-adeninate bio-MOF.

81, initial dye concentration = 10 ppm, agitation speed = 300 rpm, and solution temperature = 23°C.

3. Results and Discussion

3.1. Characterization of the Fabricated Zn-Adeninate Bio-MOF. The FT-IR spectrum of the prepared Zn-adeninate bio-MOF exhibited various characteristic peaks of both the organic framework ligands and metal. The C–O stretching peak of the carboxylic unit in the adeninate group was observed at 1600 cm^{-1} , as shown in Figure 2. The peak at 1373 cm^{-1} accounts for the C–C stretching; additionally, most bands in the range of $3000\text{--}3800\text{ cm}^{-1}$ were assigned to the OH unit of carboxylic acid [34]. The stretching frequencies of the N–H group of adenine are located in the range of $3117\text{--}3338\text{ cm}^{-1}$ [35]. The peaks observed in the wavenumber range of $420\text{--}1000\text{ cm}^{-1}$ are characteristic of the Zn–O bonds, confirming the presence of metal in the synthesized bio-MOF [36]. Therefore, the FT-IR spectrum contains the characteristic peaks of the synthesized Zn-adeninate bio-MOF.

The crystalline structure of the prepared Zn-adeninate bio-MOF was determined using XRD, as shown in Figure 3. The XRD pattern contains distinct Zn-adeninate bio-MOF peaks at 6.5° , 13.6° , and 21.8° , which can be attributed to the (111), (222), and (440) planes, respectively. These peaks are characteristic of the crystalline structure of bio-MOF and are completely different from the XRD patterns of ZnO [12, 37].

The chemical structure of the synthesized Zn-adeninate bio-MOF was investigated using XPS (Figure 4). The four peaks located at 284.2, 400, 531.6, and 1022.3 eV were assigned to C 1s, N 1s, O 1s, and Zn 2p, respectively. The C 1s spectra contained three peaks at binding energies (BE) of

284.2, 286.3, and 288.2 eV, which were related to the C=C, C=O, and COO^-/COOH functional groups, respectively [35]. The N 1s peak in the XPS spectrum of the synthesized Zn-adeninate bio-MOF indicated the presence of $-\text{NH}_2$ and $-\text{NH}_2/\text{NH}_3^+$ units [38]. Moreover, the N 1s peak characteristic of the $-\text{NH}_2$ species appeared at 399.3 eV, while the peaks corresponding to the H-bonded and/or quaternary ammonium structures were present at approximately 400 eV [1]. The O 1s spectrum contained the characteristic peak of the bridging hydroxyl ($\mu_3\text{-OH}$) group at 533 eV, while the Zn carboxylate and ($\mu_3\text{-O}$) in Zn–O peaks appeared at 531.6 eV and 531.4 eV, respectively [39]. The presence of Zn was confirmed by the appearance of Zn 2p peaks at 1022.3 and 1045.5 eV [35].

The morphology of the Zn-adeninate bio-MOF was analyzed using SEM, HRTEM, and SAED, as shown in Figure 5. The presence of large crystals in the SEM image was attributed to the agglomeration of the particles, which was proved *via* TEM. The SEM and TEM images confirmed the presence of uniform morphology with small nanoparticles in the synthesized Zn-adeninate bio-MOF sample, which was different from the extensive size distribution at the microscale observed in the previously prepared bio-MOFs. The reduction in the particle size of the synthesized sample can be attributed to the variations in the synthesis conditions, such as the long stirring time that results in the formation of smaller nanoparticles with a higher yield compared to the procedures previously described in the literature [40]. Moreover, the circular pattern observed in the SAED image revealed the homogeneous polycrystalline nature of the synthesized Zn-adeninate bio-MOF, which is in agreement with the XRD data.

The surface properties of the synthesized Zn-adeninate bio-MOF before and after the adsorption of different dyes were determined using the Brunauer-Emmett-Teller (BET) method and N_2 isotherms, as shown in Figure 6. The isotherms before and after adsorption were type III with relatively similar shapes, exhibiting an indistinct hysteresis loop related to N_2 condensation in the mesopores [41]. The specific surface area, mean pore diameter, and total pore volume of the prepared Zn-adeninate bio-MOF were approximately $52.62\text{ m}^2\text{ g}^{-1}$, 14.454 nm , and $0.183\text{ cm}^3\text{ g}^{-1}$, respectively. The large pore size and surface area of Zn-adeninate bio-MOF are appropriate for the utilization of the synthesized bio-MOF as an adsorbent for water pollutants [1]. After the adsorption process, the BET surface area of Zn-adeninate bio-MOF decreased to $34.06\text{ m}^2\text{ g}^{-1}$ and $32.59\text{ m}^2\text{ g}^{-1}$ for MB and DR-81, respectively. This was expected because of the agglomeration and blockage of pores in Zn-adeninate bio-MOF after the adsorption of MB and DR-81 ions [42].

The thermal profile of the synthesized Zn-adeninate bio-MOF was obtained in a nitrogen gas atmosphere to test its thermal stability. Multiple degradation stages are present in the thermogram of the synthesized bio-MOF, as shown in Figure 7. The first weight loss of approximately 17.5% occurred at 298°C , which can be assigned to the loss of gases and water molecules that penetrated the pores of bio-MOF [1, 33]. The second weight loss stage is approximately 59% occurred in the temperature range of $298\text{--}510^\circ\text{C}$, which

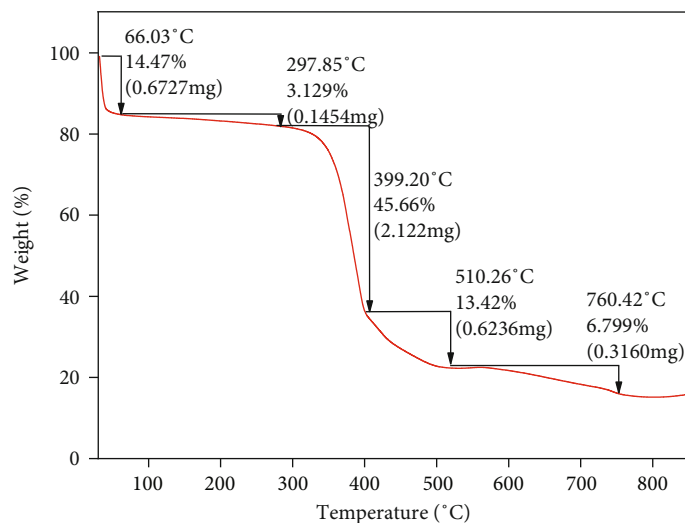


FIGURE 7: TGA plot of the synthesized Zn-adeninate bio-MOF.

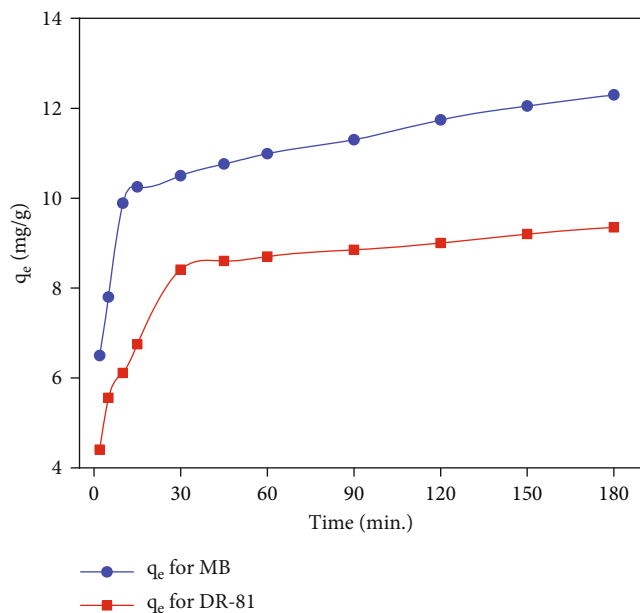


FIGURE 8: Effect of contact time on the adsorption capacity of the synthesized Zn-adeninate bio-MOF for the MB and DR-81 dyes (pH = 7, bio-MOF dosage = 1 g L⁻¹, initial concentration = 10 ppm, solution temperature = 23°C, and stirring speed = 300 rpm).

is related to the breakdown of the organic framework of the bio-MOF. These results demonstrated the excellent thermal stability of the prepared Zn-adeninate bio-MOF.

3.2. Assessment of the Synthesized Zn-Adeninate Bio-MOF for Cationic and Anionic Decolorization from Wastewater.

The performance of the prepared Zn-adeninate bio-MOF was investigated for the decolorization of MB and DR-81 from the polluted synthetic solutions at room temperature via a batch technique.

3.2.1. Influence of Contact Time on the Decolorization of Cationic and Anionic Dyes.

The effect of the contact time

on the adsorption capacity of the synthesized Zn-adeninate bio-MOF for MB and DR-81 was evaluated at different time intervals of up to 180 min, as shown in Figure 8. The adsorption capacities increased with time until the equilibrium state was reached. The improvement in the adsorption capacities for the cationic and anionic dyes in the initial stage can be attributed to the functional groups that can bind with the target dyes and large surface area of the Zn-adeninate bio-MOF [1, 12]. The optimum contact time at neutral pH was 10 min for MB and 30 min for DR-81 with adsorption capacities of 9.88 and 8.41 mg g⁻¹ for MB and DR-81, respectively. After equilibrium was achieved, the active sites of the prepared adsorbent became saturated with MB and DR-81, limiting further removal [13]. These results demonstrated the high capacity of the synthesized Zn-adeninate bio-MOF to decolorize both anionic and cationic dyes in short contact times.

3.2.2. Influence of Initial pH on the Decolorization of Cationic and Anionic Dyes.

The pH plays a significant role in the dye decolorization from wastewater. The pH directly affects the surface charge of the adsorbent and ionization degree of the pollutants [12, 43]. The pHPZC of Zn-adeninate bio-MOF was 7.2, as shown in Figure 9(a). This illustrates that the synthesized Zn-adeninate bio-MOF is positively charged till pH = 7.2 and negatively charged beyond this point [12]. The effect of pH on the decolorization process was studied at pH values ranging from 1 to 11. As shown in Figure 9(b), the acidic media were a promising candidate for decolorizing anionic DR-81 using Zn-adeninate bio-MOF. High decolorization values were recorded for the removal of DR-81 up to pH = 7, with an adsorption capacity of 8.41 mg g⁻¹, which then decreased to 3.13 mg g⁻¹ at pH = 11. By contrast, basic, neutral, and slightly acidic media favored MB decolorization. The adsorption capacity for MB decolorization was 9.89 mg g⁻¹ at pH = 7. As the pH of the solution increased to 11, the adsorption capacity of bio-MOF for MB reached 10.88 mg g⁻¹. Under alkaline conditions (pH > 7), more

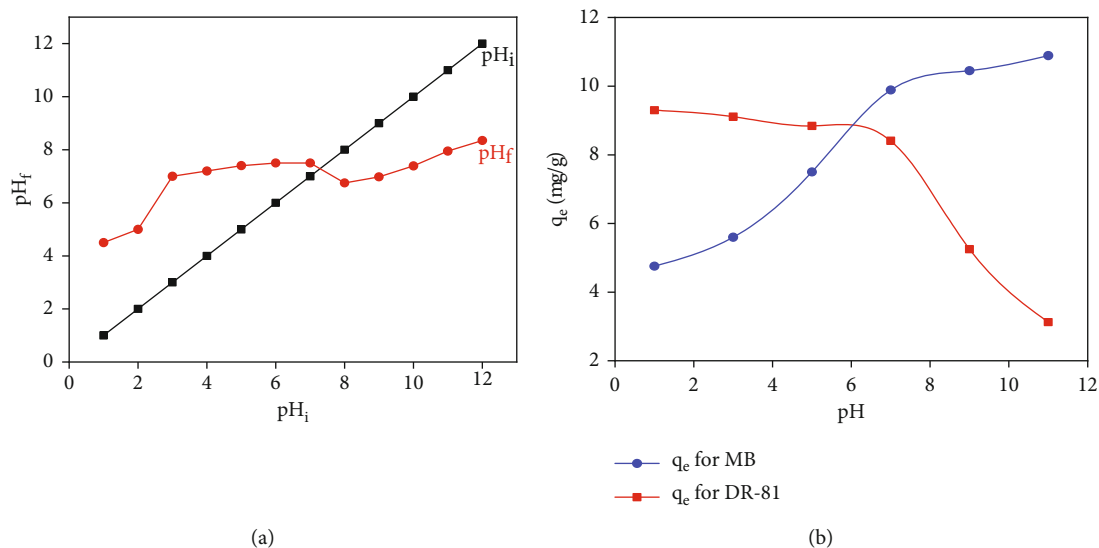


FIGURE 9: (a) The pH_{pzc} of the synthesized Zn-adeninate bio-MOF and (b) the effect of pH on the adsorption capacity of the synthesized Zn-adeninate bio-MOF for MB and DR-81 (contact time = 10 min for MB and 30 min for DR-81, bio-MOF dosage = 1 g L^{-1} , initial dye concentration = 10 ppm, stirring speed = 300 rpm, and solution temperature = 23°C) (b).

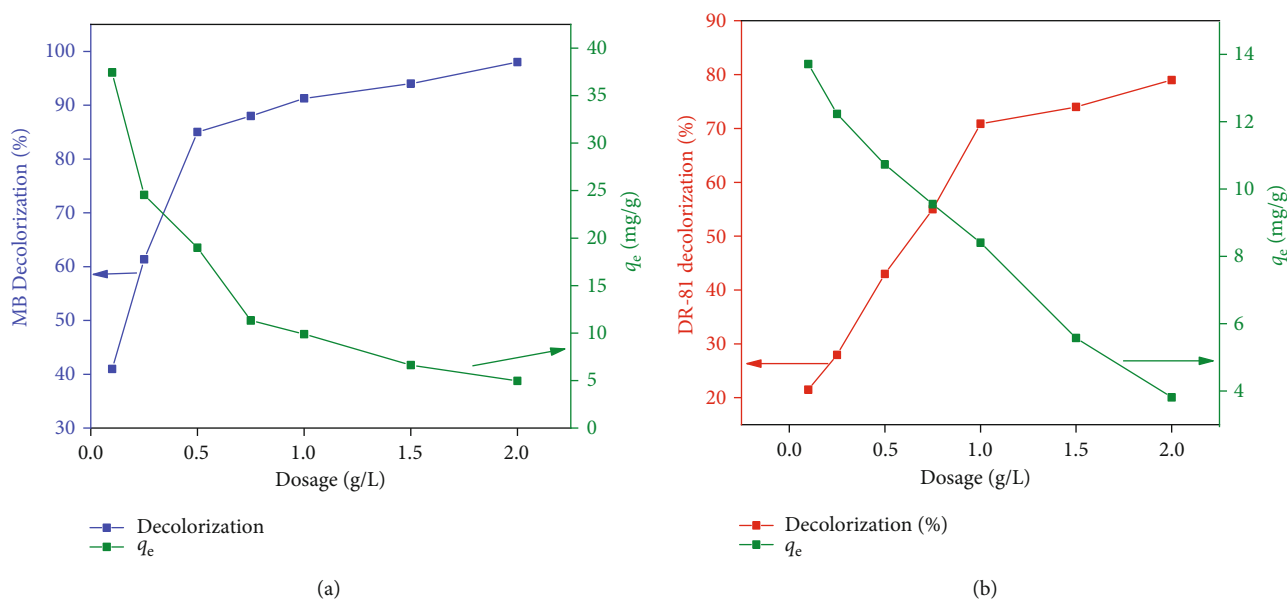


FIGURE 10: Influence of the dosage of the synthesized Zn-adeninate bio-MOF on the decolorization of (a) MB and (b) DR-81 (contact time = 10 min for MB and 30 min for DR-81, $pH = 7$, initial dye concentration = 10 ppm, stirring speed = 300 rpm, and solution temperature = 23°C).

negative ions are available in the solution; therefore, the electrostatic attractive forces between the negatively charged hydroxyl and carbonyl groups of the synthesized Zn-adeninate bio-MOF and the positively charged species of the cationic MB dye increase. Under similar conditions, repulsive forces exist between the negatively charged Zn-adeninate bio-MOF and anionic DR-81 [44]. Under acidic conditions ($pH < 7$), more protons are formed, which increase the competition with the active sites of bio-MOF, decreasing the removal of MB and increasing the removal of DR-81 [45, 46]. However, the decolorization rate of the MB dye by bio-

MOF was limited to less than 8% when the solution pH was increased from 7 to 11. Therefore, a solution pH of 7 was selected as the optimum pH for removing both DR-81 and MB dyes using the prepared Zn-adeninate bio-MOF [47].

3.2.3. Influence of the Synthesized Zn-Adeninate Bio-MOF Dosage on the Decolorization of Cationic and Anionic Dyes. The adsorbent dosage is an important factor that controls the adsorbent capacity and, hence, the decolorization process [43]. The effect of the adsorbent dosage of the synthesized Zn-adeninate bio-MOF was tested after 10 and

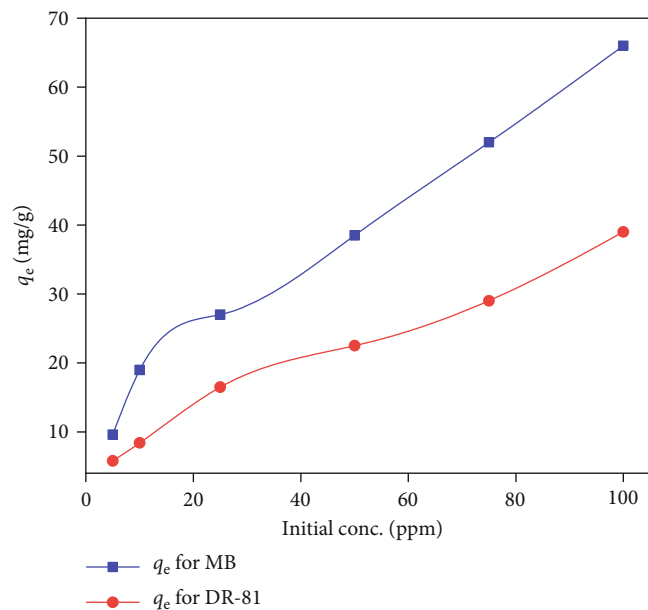


FIGURE 11: Effect of initial concentrations of the dyes on the adsorption capacity of the fabricated Zn-adeninate bio-MOF for MB and DR-81 (contact time = 10 min for MB and 30 min for DR-81, pH = 7, bio-MOF dosage = 0.5 g L^{-1} for MB and 1 g L^{-1} for DR-81, stirring speed = 300 rpm, and solution temperature = 23°C).

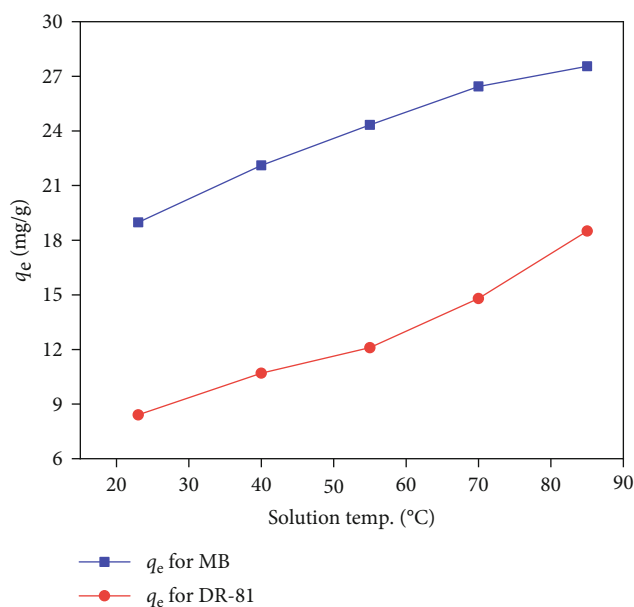


FIGURE 12: Effect of the solution temperature on the adsorption capacity of the synthesized Zn-adeninate bio-MOF for MB and DR-81 (contact time = 10 min for MB and 30 min for DR-81, pH = 7, bio-MOF dosage = 0.5 g L^{-1} for MB and 1 g/L for DR-81, initial dye concentration = 10 ppm, and stirring speed = 300 rpm).

30 min for MB and DR-81, respectively. The decolorization of MB and DR-81 dyes by the synthesized Zn-adeninate bio-MOF was enhanced by increasing the material dosages

TABLE 1: Thermodynamic parameters for the decolorization of MB and DR-81 by the synthesized Zn-adeninate bio-MOF.

Dye	ΔG° (kJ mol^{-1})	E_a (kJ mol^{-1})	ΔH° (kJ mol^{-1})	ΔS° (kJ mol^{-1})
MB	-17.70	48.02	31.27	29.22
DR-81	-3.65	35.23	34.27	36.34

from 0.1 g to 2 g L^{-1} , as shown in Figure 10. Furthermore, the decolorization capacity of the synthesized Zn-adeninate bio-MOF toward the two different dyes decreased with the increasing amounts of the synthesized adsorbent. The reduced decolorization capacity toward numerous types of dyes at high dosages of the prepared bio-MOF can be attributed to the unsaturated decolorization residual sites on the synthesized bio-MOF [1]. By contrast, increasing the dosage of the synthesized bio-MOF enabled the extra active sites available for dye decolorization, which in turn increased the removal percentage of the dyes from the wastewater. These findings can be attributed to the high surface area of the fabricated Zn-adeninate bio-MOF [48]. Therefore, the optimum dosages (or the economical dosages) of the synthesized Zn-adeninate bio-MOF were chosen as 0.5 and 1 g L^{-1} for the decolorization of MB and DR-81 dyes, respectively.

3.2.4. Influence of Initial Concentrations of the Dyes on the Decolorization Processes. The effect of the initial dye concentration on the decolorization process was investigated in the concentration range of 5 to 100 ppm at the optimum contact time, pH, and material dosage for each dye solution. Figure 11 shows that the adsorption capacity increased as the initial dye concentration increased from 5 to 100 ppm, which agrees with the results of the previous investigations [12, 49]. This may be attributed to the saturation of the surface-active sites of the adsorbent at high initial concentrations of the MB and DR-81 dyes. These results indicated that the synthesized Zn-adeninate bio-MOF possesses practical and effective ability to decolorize the cationic and anionic dyes from the wastewater at different initial dye concentrations.

3.2.5. Influence of Solution Temperature on the Decolorization of Cationic and Anionic Dyes. Figure 12 shows the influence of the solution temperature on the decolorization of the MB and DR-81 dyes by the synthesized Zn-adeninate bio-MOF. When the solution temperatures were increased from 23 to 85°C , the decolorization processes were enhanced, indicating a favorable decolorization process at high temperatures. These results indicated that the decolorization processes by the fabricated Zn-adeninate bio-MOF are endothermic [1].

3.2.6. Thermodynamic Modeling of the Decolorization Processes. The decolorization mechanism in terms of favorability, energy, and reversibility was studied and analyzed using the decolorization thermodynamics. To determine the thermodynamics of the decolorization process, the changes in enthalpy (ΔH°), entropy (ΔS°), and free energy

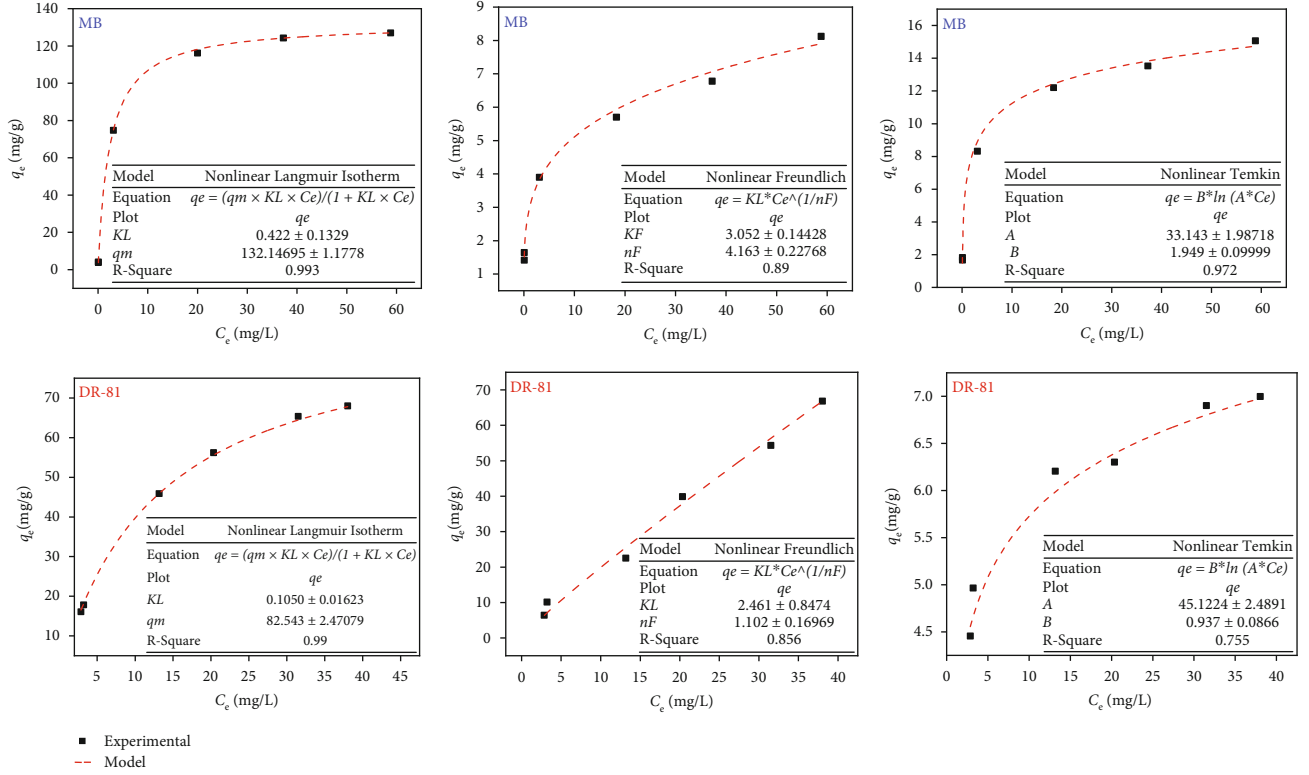


FIGURE 13: Adsorption isotherms for MB and DR-81 by the synthesized bio-MOF.

TABLE 2: Isotherm parameters of the Langmuir, Freundlich, and Temkin models for the decolorization of MB and DR-81 by the synthesized bio-MOF.

Isotherm parameters		MB	DR-81
Langmuir parameters	q_m (mg g^{-1})	132.147	82.543
	K_L (L mg^{-1})	0.422	0.105
	R_L	0.056	0.079
	R^2	0.993	0.990
Freundlich parameters	K_F (mg g^{-1})	3.052	2.461
	n_F	4.163	1.102
	R^2	0.890	0.856
Temkin parameters	A (L g^{-1})	33.143	45.1224
	B (J mol^{-1})	1.949	0.937
	R^2	0.972	0.755

(ΔG°) were determined in kilojoule per mole. The Gibbs free energy was calculated using the following equation:

$$\Delta G^\circ = -RT \ln K_c, \quad (3)$$

where T denotes the temperature of the solution in Kelvin, K_c denotes the fraction adsorbed at equilibrium, $K_c = F_e / (1 - F_e)$, $F_e = (C_0 - C_e) / C_0$, and R represents the universal gas constant ($8.314 \text{ J mol}^{-1} \text{ K}^{-1}$).

The standard entropy and enthalpy values were calculated using the Van't Hoff equation as

$$\ln K_c = \frac{\Delta S^\circ}{R} - \frac{\Delta H^\circ}{RT}. \quad (4)$$

The Hoff plot for $\ln K_c$ versus $1000/T$ was a straight line with satisfactory values of R^2 for different concentrations of MB and DR-81. The ΔS° and ΔH° values were calculated from the intercept and slope of the plot, respectively. The activation energy (E_a) was estimated using the following equation [33]:

$$E_a = \Delta H^\circ + RT. \quad (5)$$

The values of the thermodynamic parameters (E_a , ΔG° , ΔS° , and ΔH°) for the decolorization of MB and DR-81 dyes by the synthesized Zn-adeninate bio-MOF at 396 K are listed in Table 1. The negative value of ΔG° indicates that the decolorization of MB and DR-81 by the synthesized bio-MOF is thermodynamically spontaneous [14]. However, the positive value of enthalpy indicates that the decolorization processes were endothermic. Furthermore, enhanced disorder at the liquid/solid interface during the decolorization processes is reflected by the positive values of the entropy [12, 14].

3.2.7. Equilibrium Isotherms of MB and DR-81 Decolorization. To examine the decolorization behaviors of the MB and DR-81 dyes by the synthesized bio-MOF, three models, namely,

TABLE 3: Comparison of the monolayer decolorization capacities of MB and DR-81 for different nanoadsorbents.

Pollutant	Adsorbents	Optimized conditions	Decolorization capacity (mg g ⁻¹)	References
MB	Zn-adeninate bio-MOF	Time = 10 min Dosage = 0.5 g L ⁻¹ MB conc. = 10 ppm	132.15	Present study
	Activated carbon	Time = 120 min Dosage = 0.5 g L ⁻¹ MB conc. = 10 ppm	53.90	[47]
	MIP-202 bio-MOF	Time = 8 min Dosage = 1.0 g L ⁻¹ MB conc. = 10 ppm	79.79	[1]
	Cu-BTC MOF	Time = 20 min Dosage = 0.5 g L ⁻¹ MB conc. = 10 ppm	15.28	[54]
	UiO-66 MOF	Time = 20 min Dosage = 0.1 g L ⁻¹ MB conc. = 20 ppm	13.2	[55]
	Fe-BDC MOF	Time = 300 min Dosage = 2.5 g L ⁻¹ MB conc. = 5 ppm	8.65	[56]
	Zn-adeninate bio-MOF	Time = 30 min Dosage = 1.0 g L ⁻¹ DR-81 conc. = 10 ppm	82.54	Current study
DR-81	Kaolinite	Time = 120 min Dosage = 4 g L ⁻¹ DR-81 conc. = 50 ppm	26.55	[57]
	MIP-202 bio-MOF	Time = 12 min Dosage = 1.0 g L ⁻¹ DR-81 conc. = 50 ppm	36.07	[1]
	Potato peel	Time = 50 min Dosage = 0.25 g L ⁻¹ DR-81 conc. = 50 ppm	10.40	[58]
	Neem bark	Time = 50 min Dosage = 0.25 g L ⁻¹ DR-81 conc. = 50 ppm	8.40	[58]

Langmuir, Freundlich, and Temkin, were utilized. For nonlinear estimation, a trial-and-error method was developed to minimize the error distribution between the experimental and theoretical adsorption data using the Solver add-in of Microsoft Excel. The Langmuir nonlinearized plots exhibited good correlation coefficients ($R^2 = 0.993$ for MB and 0.990 for DR-81) [50].

$$q_e = \frac{q_m K_L C_e}{1 + K_L C_e}, \quad (6)$$

where C_e refers to the adsorbate equilibrium concentration (mg L⁻¹), q_e denotes the adsorbed amount of MB/DR-81 at equilibrium (mg g⁻¹), and K_L and q_m denote the Langmuir constants of the decolorization energy (L mg⁻¹) and maximum

monolayer decolorization capacity (mg g⁻¹), respectively. Equation (7) was used to test the Freundlich model by plotting $\log q_e$ against $\log C_e$ [51].

$$q_e = K_F \times C_e^{1/n_f}, \quad (7)$$

where K_F and n_f denote the Freundlich constants related to the capacity and intensity of decolorization, respectively. Equation (8) was employed to verify the Temkin isotherm model for the adsorption data of the MB and DR-81 dyes on bio-MOF [52].

$$q_e = \left(\frac{RT}{b}\right) \ln(A \times C_e), \quad (8)$$

TABLE 4: Parameters of the kinetic models for MB and DR-81 removal by the synthesized Zn-adeninate bio-MOF.

Kinetic model	Parameters	MB	DR-81
Pseudo-first-order model	$q_{\text{exp.}}$ (mg g^{-1})	17.992	11.835
	q_{theor} (mg g^{-1})	1.842	6.328
	K_1 (min^{-1})	0.274	0.250
	R^2	0.531	0.463
Pseudo-second-order model	$q_{\text{exp.}}$ (mg g^{-1})	17.992	11.834
	q_{theor} (mg g^{-1})	18.134	12.008
	K_2 (g min mg^{-1})	0.437	0.111
	R^2	0.996	0.989
Elovich kinetic model	α (mg min g^{-1})	12.426	7.252
	β (g mg^{-1})	0.0921	0.447
	R^2	0.800	0.679
	C_1 ($\text{mg g}^{-1} \text{min}^{-1}$)	19.751	10.341
Intraparticle diffusion kinetic model	k_i (g mg^{-1})	0.022	0.362
	R^2	0.700	0.790

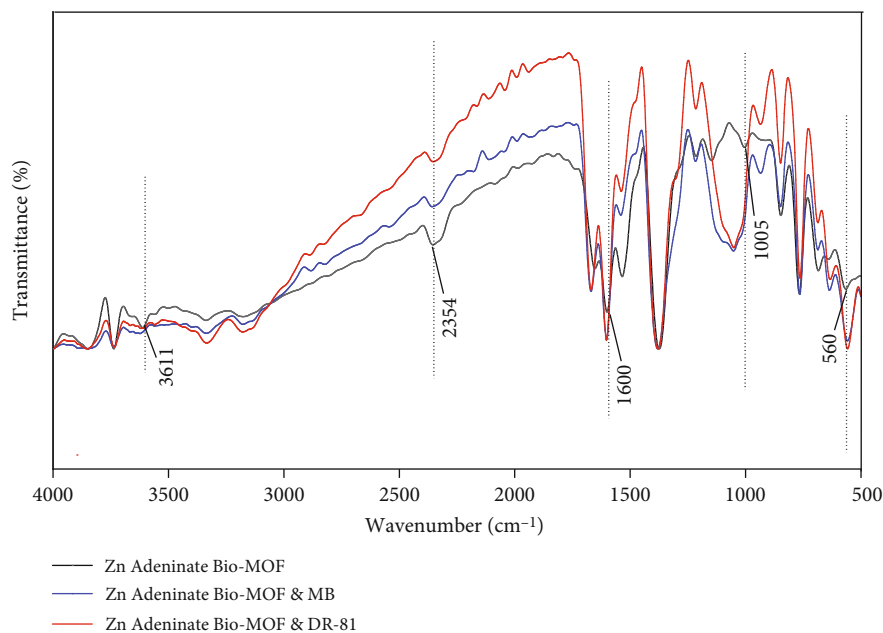


FIGURE 14: Comparison of the FT-IR spectra of (a) the synthesized Zn-adeninate bio-MOF, (b) Zn-adeninate bio-MOF and MB, and (c) Zn-adeninate bio-MOF and DR-81.

where $B = RT/b$ is a constant that is related to the decolorization heat (J mol^{-1}) and A is the Temkin isotherm constant (L g^{-1}).

A comparison of the nonlinear fittings of the Langmuir, Freundlich, and Temkin models is presented in Figure 13 and Table 2.

The Langmuir model was found to be the most appropriate for describing the dye removal processes of MB and DR-81 by the synthesized bio-MOF because this model showed the highest correlation coefficients. Additionally,

the values of the separation factor R_L were in the range of 0 to 1, which indicated that the Langmuir model is favorable for describing the dye removal procedures [53]. Meanwhile, the Freundlich decolorization intensities (n_F) were 4.163 and 1.102 for the decolorization of MB and DR-81, respectively, which was higher than unity, indicating the favorable nature of dye removal by the synthesized adsorbent [1, 53]. By contrast, the Temkin correlation coefficients had low values, indicating poor fitting of the equilibrium decolorization data of MB and DR-81 with the Temkin isothermal model.

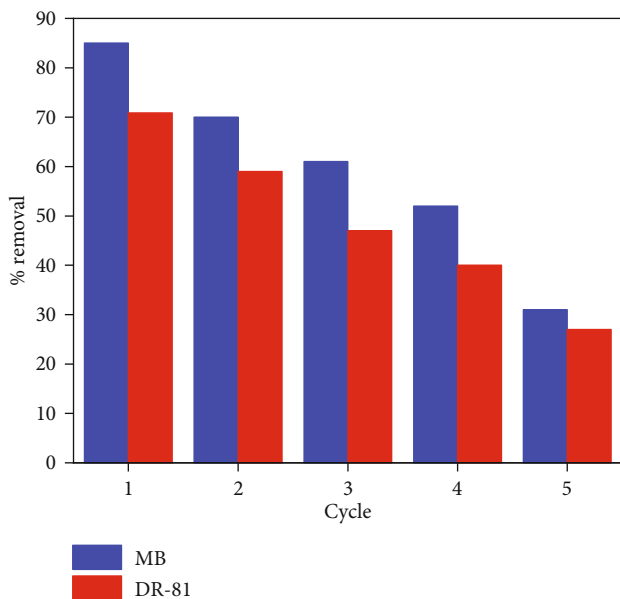


FIGURE 15: Reusability test of the synthesized Zn-adeninate bio-MOF against cationic and anionic dyes.

Hence, the Langmuir model was found to be the most suitable for describing the monolayer decolorization of MB and DR-81 by the synthesized bio-MOF surface [43].

3.2.8. Comparison of the Decolorization Capacity of MB and DR-81 for the Synthesized Zn-Adeninate Bio-MOF with other Adsorbents. The monolayer decolorizing capacities (q_m) of the MB and DR-81 dyes for Zn-adeninate bio-MOF were compared with the q_m values of other reported nanoadsorbents (Table 3). The synthesized Zn-adeninate bio-MOF was found to have better decolorization results for MB and DR-81 compared to those of the previously reported nanoadsorbents.

3.2.9. Decolorization Kinetic Analysis of the MB and DR-81 Dyes. Pseudo-first-order and pseudo-second-order models were used to understand the decolorization kinetics of MB and DR-81 by the synthesized Zn-adeninate bio-MOF. The two nonlinear decolorization models can be described by Equations (9) and (10), respectively [59, 60]:

$$q_t = q_e \left(1 - e^{-k_1 t}\right), \quad (9)$$

$$q_t = \frac{q_e^2 K_2 t}{q_e K_2 t + 1}, \quad (10)$$

where q_t and q_e (mg g^{-1}) denote the adsorbed amounts of dye at time t and equilibrium, respectively, and K_1 (min^{-1}) and K_2 ($\text{g mg}^{-1} \text{min}^{-1}$) define the rate constants of the pseudo-first-order and pseudo-second-order models, respectively. Additionally, the following nonlinear Elovich equation was used to decolorize the different water pollutants [61]:

$$q_t = \left(\frac{1}{\beta}\right) \ln(1 + \alpha \beta t), \quad (11)$$

where α denotes the initial decolorization rate ($\text{mg g}^{-1} \text{min}^{-1}$) and β is related to the degree of surface coverage and decolorization activation energy (g mg^{-1}). The intercept and slope of the linear plot of q_t versus $\ln t$ describe β and α , respectively. The intraparticle diffusion model was explored using the following equation proposed by Weber and Morris [62]:

$$q_t = k_i t^{1/2} + C, \quad (12)$$

where k_i denotes the constant of the intraparticle diffusion rate and C denotes the thickness of the border layer. The linear fitting of q_t versus $t^{1/2}$ when the plot passes through the origin indicates intraparticle diffusion, in which the rate-limiting process is the only intraparticle diffusion process. If this was not obtained, other mechanisms along with the intraparticle diffusion would be included.

The correlation coefficients of the four kinetic models are listed in Table 4. The nonlinearity of q_t versus time plots show high correlation coefficient values of 0.996 and 0.989 for the MB and DR-81 dyes, respectively. The computed q_e values were in perfect agreement with the experimental data (q_e) for the pseudo-second-order kinetics. Hence, the decolorization of MB and DR-81 by the synthesized bio-MOF followed the pseudo-second-order kinetic model. According to the pseudo-second-order model, the decolorization processes become rapid and equilibrium times are very short, which is similar to the experimental results. Rapid adsorption of MB and DR-81 on Zn-adeninate bio-MOF occurred in the first 25 min, and then, it diminished in the subsequent 3 h. The rapid adsorption can be principally associated with boundary layer diffusion or macropore diffusion, while the reluctant decolorization is due to intraparticle diffusion or micropore diffusion with a low R^2 value [63]. The data confirmed that MB and DR-81 decolorization processes by the synthesized bio-MOF may be mainly controlled by a pseudo-second-order model for the studied pollutants [1, 14].

3.2.10. Decolorization Mechanism of MB and DR-81 by the Synthesized Bio-MOF. The FT-IR spectra before and after the decolorization of MB and DR-81 were compared, as shown in Figure 14. Following MB and DR-81 adsorption, the FT-IR spectra showed distinct changes due to the decolorization of the cationic and anionic dyes by the Zn-adeninate bio-MOF. The transition in the peak at 1005 cm^{-1} may be due to the symmetric bending of S-O in MB with Zn bio-MOF. Furthermore, the variation in the characteristic peak at 1600 cm^{-1} may be due to the chemical combination of C-C in Zn bio-MOF with the electrophilic N^+ groups of DR-81 and MB [1]. Furthermore, the Zn-O peak in the lower wavenumber region shifted, indicating the interaction between Zn-O and the positively charged groups in the dyes [64]. The characteristic peak of the asymmetric vibration at 3611 cm^{-1} shifted, indicating chemical bonding between the $-\text{NH}_2$ group and positively charged

functional groups of the dyes [36]. These findings indicated that the decolorization mechanism of the MB and DR-81 dyes by the synthesized Zn-adeninate bio-MOF might be chemically controlled.

3.2.11. Recyclability Study of the Synthesized Zn-Adeninate Bio-MOF. The regeneration of the adsorbent is significant because it affects the cost of practical applications [1, 14]. The synthesized adsorbent was washed and reused to decolorize MB and DR-81 from wastewater. The decolorization-desorption cycles were repeated five times, as shown in Figure 15. The results indicated that the prepared Zn-adeninate bio-MOF could be reused several times with high decolorization performance for both MB and DR-81 [1].

4. Conclusions

In this study, a novel, efficient, environmentally benign, and nontoxic adsorbent of porous Zn-adeninate bio-MOF was reported for the decolorization of both cationic and anionic dyes from wastewater. The prepared Zn-adeninate bio-MOF was characterized using different techniques, such as XRD, FT-IR, BET, SEM, TEM, XPS, and TGA. The synthesized Zn-adeninate bio-MOF had a surface area of $52.62 \text{ m}^2 \text{ g}^{-1}$ and total pore volume of $0.183 \text{ cm}^3 \text{ g}^{-1}$. The decolorization processes of the MB and DR-81 dyes were in agreement with the Langmuir model, which represents monolayer decolorization by the prepared Zn bio-MOF. The best-fit kinetic model for the MB and DR-81 dye decolorization was the pseudo-second-order model. Furthermore, the maximum decolorization capacity of the synthesized Zn-adeninate bio-MOF against MB and DR-81 was 132.15 and 82.54 mg g^{-1} , respectively. The synthesized Zn-adeninate bio-MOF could be reused several times with a high decolorization performance. Accordingly, the prepared Zn-adeninate bio-MOF is a promising and effective adsorbent for MB and DR-81 from wastewater, with high stability and good reusability for numerous cycles.

Data Availability

All the investigated data in this study are included in the submitted article.

Conflicts of Interest

The authors declare no conflicts of interest.

Acknowledgments

This work was supported by the Science, Technology & Innovation Funding Authority (STDF) (grant number 43565).

References

[1] K. E. Diab, E. Salama, H. S. Hassan, A. Abd El-moneim, and M. F. Elkady, "Biocompatible MIP-202 Zr-MOF tunable sorbent for cost-effective decontamination of anionic and cationic

pollutants from waste solutions," *Scientific Reports*, vol. 11, no. 1, pp. 1–13, 2021.

[2] X. Li, B. Wang, Y. Cao et al., "Water contaminant elimination based on metal–organic frameworks and perspective on their industrial applications," *ACS Sustainable Chemistry & Engineering*, vol. 7, no. 5, pp. 4548–4563, 2019.

[3] H. Yuan, L. Chen, Z. Cao, and F. F. Hong, "Enhanced decolorization efficiency of textile dye Reactive Blue 19 in a horizontal rotating reactor using strips of BNC-immobilized laccase: optimization of conditions and comparison of decolorization efficiency," *Biochemical Engineering Journal*, vol. 156, article 107501, 2020.

[4] S. Ledakowicz and K. Paździor, "Recent achievements in dyes removal focused on advanced oxidation processes integrated with biological methods," *Molecules*, vol. 26, no. 4, p. 870, 2021.

[5] A. Albahnasawi, E. Yüksel, E. Gürbulak, and F. Duyum, "Fate of aromatic amines through decolorization of real textile wastewater under anoxic-aerobic membrane bioreactor," *Journal of Environmental Chemical Engineering*, vol. 8, no. 5, article 104226, 2020.

[6] R. Kant, "Textile dyeing industry an environmental hazard," *Natural Science*, vol. 4, article 17027, p. 5, 2012.

[7] P. Bajpai, *Pulp and Paper Industry: Chemicals*, Elsevier, Amsterdam, 2015.

[8] V. Gupta, I. A. Suhas, and V. Saini, "Removal of rhodamine B, fast green, and methylene blue from wastewater using red mud, an aluminum industry waste," *Industrial & Engineering Chemistry Research*, vol. 43, no. 7, pp. 1740–1747, 2004.

[9] O. S. Bayomie, H. Kandeel, T. Shoeb, H. Yang, N. Youssef, and M. M. El-Sayed, "Novel approach for effective removal of methylene blue dye from water using fava bean peel waste," *Scientific Reports*, vol. 10, no. 1, pp. 1–10, 2020.

[10] A. Giwa, A. Yusuf, H. A. Balogun et al., "Recent advances in advanced oxidation processes for removal of contaminants from water: a comprehensive review," *Process Safety and Environmental Protection*, vol. 146, pp. 220–256, 2021.

[11] N. Nippatla and L. Philip, "Electrocoagulation-floatation assisted pulsed power plasma technology for the complete mineralization of potentially toxic dyes and real textile wastewater," *Process Safety and Environmental Protection*, vol. 125, pp. 143–156, 2019.

[12] M. F. Elkady, H. Shokry Hassan, and E. Salama, "Sorption profile of phosphorus ions onto ZnO nanorods synthesized via sonic technique," *Journal of Engineering*, vol. 2016, Article ID 2308560, 2016.

[13] M. F. Elkady, H. S. Hassan, W. A. Amer, E. Salama, H. Algarni, and E. R. Shaaban, "Novel magnetic zinc oxide nanotubes for phenol adsorption: mechanism modeling," *Materials*, vol. 10, no. 12, p. 1355, 2017.

[14] M. Elkady, E. Salama, W. A. Amer, E.-Z. M. Ebeid, M. M. Ayad, and H. Shokry, "Novel eco-friendly electrospun nanomagnetic zinc oxide hybridized PVA/alginate/chitosan nanofibers for enhanced phenol decontamination," *Environmental Science and Pollution Research*, vol. 27, no. 34, pp. 43077–43092, 2020.

[15] K. Meerbergen, S. Crauwels, K. A. Willems et al., "Decolorization of reactive azo dyes using a sequential chemical and activated sludge treatment," *Journal of Bioscience and Bioengineering*, vol. 124, no. 6, pp. 668–673, 2017.

[16] J. Meng, Y. Xie, Y.-H. Gu et al., "PVDF-CaAlg nanofiltration membranes with dual thin-film-composite (TFC) structure

- and high permeation flux for dye removal,” *Separation and Purification Technology*, vol. 255, article 117739, 2021.
- [17] L. Cseri, F. Topuz, M. A. Abdulhamid, A. Alammari, P. M. Budd, and G. Szekely, “Electrospun adsorptive nanofibrous membranes from ion exchange polymers to snare textile dyes from wastewater,” *Advanced Materials Technologies*, vol. 6, no. 10, article 2000955, 2021.
- [18] M. Shaban, M. R. Abukhadra, A. Hamd, R. R. Amin, and A. A. Khalek, “Photocatalytic removal of Congo red dye using MCM-48/Ni₂O₃ composite synthesized based on silica gel extracted from rice husk ash; fabrication and application,” *Journal of Environmental Management*, vol. 204, no. 1, pp. 189–199, 2017.
- [19] B. Dong, H. Chen, Y. Yang, Q. He, and X. Dai, “Treatment of printing and dyeing wastewater using MBBR followed by membrane separation process,” *Desalination and Water Treatment*, vol. 52, no. 22–24, pp. 4562–4567, 2014.
- [20] O. Onukwuli, P. Nnaji, M. Menkiti et al., “Dual-purpose optimization of dye-polluted wastewater decontamination using bio-coagulants from multiple processing techniques via neural intelligence algorithm and response surface methodology,” *Journal of the Taiwan Institute of Chemical Engineers*, vol. 125, pp. 372–386, 2021.
- [21] M. Hartl, M. J. García-Galán, V. Matamoros et al., “Constructed wetlands operated as bioelectrochemical systems for the removal of organic micropollutants,” *Chemosphere*, vol. 271, article 129593, 2021.
- [22] C. Manera, A. P. Tonello, D. Perondi, and M. Godinho, “Adsorption of leather dyes on activated carbon from leather shaving wastes: kinetics, equilibrium and thermodynamics studies,” *Environmental Technology*, vol. 40, no. 21, pp. 2756–2768, 2019.
- [23] S. Dutta, B. Gupta, S. K. Srivastava, and A. K. Gupta, “Recent advances on the removal of dyes from wastewater using various adsorbents: a critical review,” *Materials Advances*, vol. 2, no. 14, pp. 4497–4531, 2021.
- [24] M. M. Ayad, W. A. Amer, S. Zaghlool, I. M. Minisy, P. Bober, and J. Stejskal, “Polypyrrole-coated cotton textile as adsorbent of methylene blue dye,” *Chemical Papers*, vol. 72, no. 7, pp. 1605–1618, 2018.
- [25] W. A. Amer, M. M. Omran, and M. M. Ayad, “Acid-free synthesis of polyaniline nanotubes for dual removal of organic dyes from aqueous solutions,” *Colloids and Surfaces A: Physicochemical and Engineering Aspects*, vol. 562, pp. 203–212, 2019.
- [26] V. K. M. Au, “Recent advances in the use of metal-organic frameworks for dye adsorption,” *Frontiers in Chemistry*, vol. 8, p. 708, 2020.
- [27] K. Wang, H. Huang, W. Xue et al., “An ultrastable Zr metal-organic framework with a thiophene-type ligand containing methyl groups,” *CrystEngComm*, vol. 17, no. 19, pp. 3586–3590, 2015.
- [28] M. S. Khan, M. Khalid, and M. Shahid, “What triggers dye adsorption by metal organic frameworks? The current perspectives,” *Materials Advances*, vol. 1, no. 6, pp. 1575–1601, 2020.
- [29] M. R. Saeb, N. Rabiee, M. Mozafari, and E. Mostafavi, “Metal-organic frameworks-based nanomaterials for drug delivery,” *Materials*, vol. 14, no. 13, p. 3652, 2021.
- [30] S. Salamat, M. Hadavifar, and H. Rezaei, “Preparation of nanochitosan-STP from shrimp shell and its application in removing of malachite green from aqueous solutions,” *Journal of Environmental Chemical Engineering*, vol. 7, no. 5, article 103328, 2019.
- [31] S. S. Nadar, L. Vaidya, S. Maurya, and V. K. Rathod, “Polysaccharide based metal organic frameworks (polysaccharide-MOF): a review,” *Coordination Chemistry Reviews*, vol. 396, pp. 1–21, 2019.
- [32] A. H. Ibrahim, W. A. El-Mehalmey, R. R. Haikal et al., “Tuning the chemical environment within the UiO-66-NH₂ nanocages for charge-dependent contaminant uptake and selectivity,” *Inorganic Chemistry*, vol. 58, no. 22, pp. 15078–15087, 2019.
- [33] H. Shokry, M. Elkady, and E. Salama, “Eco-friendly magnetic activated carbon nano-hybrid for facile oil spills separation,” *Scientific Reports*, vol. 10, no. 1, pp. 1–17, 2020.
- [34] Q. Qian, A. X. Wu, W. S. Chi et al., “Mixed-matrix membranes formed from imide-functionalized UiO-66-NH₂ for improved interfacial compatibility,” *ACS Applied Materials & Interfaces*, vol. 11, no. 34, pp. 31257–31269, 2019.
- [35] Y. Rachuri, J. F. Kurisingal, R. K. Chitumalla et al., “Adenine-based Zn(II)/Cd(II) metal-organic frameworks as efficient heterogeneous catalysts for facile CO₂ fixation into cyclic carbonates: a DFT-supported study of the reaction mechanism,” *Inorganic Chemistry*, vol. 58, no. 17, pp. 11389–11403, 2019.
- [36] T. Hashem, A. H. Ibrahim, C. Wöll, and M. H. Alkordi, “Grafting zirconium-based metal-organic framework UiO-66-NH₂ nanoparticles on cellulose fibers for the removal of Cr(VI) ions and methyl orange from water,” *ACS Applied Nano Materials*, vol. 2, no. 9, pp. 5804–5808, 2019.
- [37] J. An, O. K. Farha, J. T. Hupp, E. Pohl, J. I. Yeh, and N. L. Rosi, “Metal-adeninate vertices for the construction of an exceptionally porous metal-organic framework,” *Nature Communications*, vol. 3, no. 1, pp. 1–6, 2012.
- [38] N. Graf, E. Yegen, T. Gross et al., “XPS and NEXAFS studies of aliphatic and aromatic amine species on functionalized surfaces,” *Surface Science*, vol. 603, no. 18, pp. 2849–2860, 2009.
- [39] Y. Wang, L. Li, P. Dai et al., “Missing-node directed synthesis of hierarchical pores on a zirconium metal-organic framework with tunable porosity and enhanced surface acidity via a microdroplet flow reaction,” *Journal of Materials Chemistry A*, vol. 5, no. 42, pp. 22372–22379, 2017.
- [40] G. Han, Q. Qian, K. Mizrahi Rodriguez, and Z. P. Smith, “Hydrothermal synthesis of sub-20 nm amine-functionalized MIL-101(Cr) nanoparticles with high surface area and enhanced CO₂ uptake,” *Industrial & Engineering Chemistry Research*, vol. 59, no. 16, pp. 7888–7900, 2020.
- [41] H. Hamad, E. Bailon-Garcia, S. Morales-Torres, F. Carrasco-Marin, A. F. Perez-Cadenas, and F. J. Maldonado-Hodar, “Physicochemical properties of new cellulose-TiO₂ composites for the removal of water pollutants: developing specific interactions and performances by cellulose functionalization,” *Journal of Environmental Chemical Engineering*, vol. 6, no. 4, pp. 5032–5041, 2018.
- [42] A. M. Omer, E. M. Abd El-Monaem, M. M. Abd El-Latif, G. M. El-Subruiti, and A. S. Eltaweil, “Facile fabrication of novel magnetic ZIF-67 chitosan composite beads for the adsorptive removal of Cr(VI) from aqueous solutions,” *Carbohydrate Polymers*, vol. 265, article 118084, 2021.
- [43] M. Abd El-Latif, A. M. Ibrahim, and M. El-Kady, “Adsorption equilibrium, kinetics and thermodynamics of methylene blue from aqueous solutions using biopolymer oak sawdust composite,” *Journal of American Science*, vol. 6, no. 6, pp. 267–283, 2010.

- [44] K. Parida and A. C. Pradhan, "Removal of phenolic compounds from aqueous solutions by adsorption onto manganese nodule leached residue," *Journal of Hazardous Materials*, vol. 173, no. 1-3, pp. 758-764, 2010.
- [45] E. M. El-Sayed, H. A. Hamad, and R. M. Ali, "Journey from ceramic waste to highly efficient toxic dye adsorption from aqueous solutions via one-pot synthesis of CaSO_4 rod-shape with silica," *Journal of Materials Research and Technology*, vol. 9, no. 6, pp. 16051-16063, 2020.
- [46] A. Hamadi, N. Yeddou-Mezenner, A. Lounis, R. M. Ali, and H. Hamad, "Upgrading of agro-industrial green biomass residues from chocolate industry for adsorption process: diffusion and mechanistic insights," *Journal of Food Science and Technology*, vol. 58, no. 3, pp. 1081-1092, 2021.
- [47] Y. Kuang, X. Zhang, and S. Zhou, "Adsorption of methylene blue in water onto activated carbon by surfactant modification," *Water*, vol. 12, no. 2, p. 587, 2020.
- [48] M. El-Aassar, I. H. Alsohaimi, A. S. Ali, and A. A. Elzain, "Removal of phenol and Bisphenol A by immobilizedLaccaseon poly (acrylonitrile-co-styrene/pyrrole) nanofibers," *Separation Science and Technology*, vol. 55, no. 15, pp. 2670-2678, 2020.
- [49] M. F. Elkady, M. R. El-Aassar, and H. S. Hassan, "Adsorption profile of basic dye onto novel fabricated carboxylated functionalized co-polymer nanofibers," *Polymers*, vol. 8, no. 5, p. 177, 2016.
- [50] I. Langmuir, "The constitution and fundamental properties of solids and liquids. Part I. Solids," *Journal of the American Chemical Society*, vol. 38, no. 11, pp. 2221-2295, 1916.
- [51] H. Freundlich, "Über die adsorption in lösungen," *Zeitschrift für Physikalische Chemie*, vol. 57U, no. 1, pp. 385-470, 1907.
- [52] M. Temkin, "Kinetics of ammonia synthesis on promoted iron catalysts," *Acta physiochim. URSS*, vol. 12, pp. 327-356, 1940.
- [53] O. Üner, Ü. Geçgel, and Y. Bayrak, "Adsorption of methylene blue by an efficient activated carbon prepared from Citrullus lanatus rind: kinetic, isotherm, thermodynamic, and mechanism analysis," *Water, Air, & Soil Pollution*, vol. 227, no. 7, pp. 1-15, 2016.
- [54] S. Lin, Z. Song, G. Che et al., "Adsorption behavior of metal-organic frameworks for methylene blue from aqueous solution," *Microporous and Mesoporous Materials*, vol. 193, pp. 27-34, 2014.
- [55] J. Qiu, Y. Feng, X. Zhang, M. Jia, and J. Yao, "Acid-promoted synthesis of UiO-66 for highly selective adsorption of anionic dyes: adsorption performance and mechanisms," *Journal of Colloid and Interface Science*, vol. 499, pp. 151-158, 2017.
- [56] C. Arora, S. Soni, S. Sahu, J. Mittal, P. Kumar, and P. Bajpai, "Iron based metal organic framework for efficient removal of methylene blue dye from industrial waste," *Journal of Molecular Liquids*, vol. 284, pp. 343-352, 2019.
- [57] T. A. Khan, S. Dahiya, and E. A. Khan, "Removal of direct red 81 from aqueous solution by adsorption onto magnesium oxide-coated kaolinite: isotherm, dynamics and thermodynamic studies," *Environmental Progress & Sustainable Energy*, vol. 36, no. 1, pp. 45-58, 2017.
- [58] N. Sharma, D. Tiwari, and S. Singh, "Efficiency of chemically treated potato peel and Neem bark for sorption of Direct Red-81 dye from aqueous solution," *Rasayan Journal of Chemistry*, vol. 7, article 399e409, 2014.
- [59] S. K. Lagergren, "About the theory of so-called adsorption of soluble substances," *Sven. Vetenskapsakad. Handlingar*, vol. 24, pp. 1-39, 1898.
- [60] Y. Ho and G. McKay, "Kinetic model for lead (II) sorption on to peat," *Adsorption Science & Technology*, vol. 16, no. 4, pp. 243-255, 1998.
- [61] S. Chien and W. Clayton, "Application of Elovich equation to the kinetics of phosphate release and sorption in soils," *Soil Science Society of America Journal*, vol. 44, no. 2, pp. 265-268, 1980.
- [62] W. J. Weber Jr. and J. C. Morris, "Kinetics of adsorption on carbon from solution," *Journal of the Sanitary Engineering Division*, vol. 89, no. 2, pp. 31-59, 1963.
- [63] N. Widiastuti, H. Wu, H. M. Ang, and D. Zhang, "Removal of ammonium from greywater using natural zeolite," *Desalination*, vol. 277, no. 1-3, pp. 15-23, 2011.
- [64] K. Vikrant, V. Kumar, K.-H. Kim, and D. Kukkar, "Metal-organic frameworks (MOFs): potential and challenges for capture and abatement of ammonia," *Journal of Materials Chemistry A*, vol. 5, no. 44, pp. 22877-22896, 2017.